Generalization and Regularization for Inverse Cardiac Estimators

Francisco M. Melgarejo-Meseguer ⓘ, Estrella Everss-Villalba, Miriam Gutiérrez-Fernández-Calvillo,
Sergio Muñoz-Romero ⓘ, Francisco-Javier Gimeno-Blanes ⓘ, Arcadi García-Alberola,
and José-Luis Rojo-Álvarez ⓘ, *Senior Member, IEEE*

Abstract—Electrocardiographic Imaging (ECGI) aims to estimate the intracardiac potentials noninvasively, hence allowing the clinicians to better visualize and understand many arrhythmia mechanisms. Most of the estimators of epicardial potentials use a signal model based on an estimated spatial transfer matrix together with Tikhonov regularization techniques, which works well specially in simulations, but it can give limited accuracy in some real data. Based on the quasielectrostatic potential superposition principle, we propose a simple signal model that supports the implementation of principled out-of-sample algorithms for several of the most widely used regularization criteria in ECGI problems, hence improving the generalization capabilities of several of the current estimation methods. Experiments on simple cases (cylindrical and Gaussian shapes scrutinizing fast and slow changes, respectively) and on real data (examples of torso tank measurements available from Utah University, and an animal torso and epicardium measurements available from Maastricht University, both in the EDGAR public repository) show that the superposition-based out-of-sample tuning of regularization parameters promotes stabilized estimation errors of the unknown source potentials, while slightly increasing the re-estimation error on the measured data, as natural in non-overfitted solutions. The superposition signal model can be used for designing adequate out-of-sample tuning of Tikhonov regularization techniques, and it can be taken into account when using other regularization techniques in current commercial systems and research toolboxes on ECGI.

Index Terms—Cross Validation, electrocardiographic imaging, generalization, out-of-sample estimation, potential, quasielectrostatics superposition, regularization.

Francisco M. Melgarejo-Meseguer, Estrella Everss-Villalba, and Miriam Gutiérrez-Fernández-Calvillo are with the Department of Signal Theory and Communications and Telematic Systems and Computation, Rey Juan Carlos University, Spain.

Sergio Muñoz-Romero is with the Department of Signal Theory and Communications and Telematic Systems and Computation, Rey Juan Carlos University, Spain, and also with the D! lemma Lab Ltd Startup, Spain.

Francisco-Javier Gimeno-Blanes is with the Department of Communication Engineering, Miguel Hernández University, Spain, and also with the D! lemma Lab Ltd Startup, Spain.

Arcadi García-Alberola is with the Unidad de Arritmias, Hospital Clínico Universitario Virgen de la Arrixaca, Spain.

José-Luis Rojo-Álvarez is with the Department of Signal Theory and Communications and Telematic Systems and Computation, Rey Juan Carlos University, 28943 Fuenlabrada, Madrid, Spain, and also with the D! lemma Lab Ltd Startup, 28943 Fuenlabrada, Madrid, Spain (e-mail: joseluis.rojo@urjc.es).

I. INTRODUCTION

CARDIOVASCULAR diseases, including those related with cardiac arrhythmias, remain as the most common cause of death in developed countries [1], [2]. Arrhythmias are often associated to cardiovascular diseases, either as a primary etiologic factor or as a complication of a preexisting disease, with potentially serious symptomatic, prognostic, and therapeutic implications. Some arrhythmias have well known and simple mechanisms that allow a relatively easy therapeutic approach with catheter ablation techniques. In contrast, other arrhythmias such as the fibrillatory rhythms seem to involve complex bioelectrical, anatomical, and pathophysiological mechanisms, many of them not yet clearly understood, which makes difficult the development of successful ablation strategies. Electrocardiographic Imaging (ECGI) is receiving special attention today, and this non-invasive mapping allows the cardiologists to characterize and visualize the spatial-temporal activity of potentials in the cardiac tissue, both for atrial and ventricular originated arrhythmias [3]–[5]. A significant number of studies suggest and support the clinical utility of ECGI in knowing and locating more precisely the underlying mechanisms of arrhythmias [6]–[8].

ECGI systems always include an algorithm for solving the inverse problem, whose solution is an estimation of the potentials on the heart that are originating a set of potentials measured on the torso. For this purpose, a number of algorithms have been proposed in the literature based on mathematical models of cardiac electrophysiology of the forward problem [9]. Two main requirements are needed to solve the inverse problem in ECGI: First, we require a mathematical and geometric description of the volume tissue, through which the potential field runs from the cardiac source to the torso sensors; And second, actual signals have to be measured at an appropriate sampling rate (from 500

to 2000 samples per second), and the exact positions where they were recorded need to be known [10], [11].

From a numerical point of view, estimation methods typically have to deal with several hundred to a few thousand signals in the presence of different noise sources, thus requiring stabilization in their solution by using the so-called regularization techniques. The scientific literature includes a good number of methods to address the regularization in the inverse problem, among which we can mention Tikhonov regularization (with zero, first, or second order), Generalized Minimal REsiduals (GMRE), Truncated Singular Value Decomposition (TSVD), Total Variation (TV), Bayesian Maximum a Posteriori Estimation, and MUltiple Signal Classification (MUSIC), among others. Without entering into relevant numerical details, we can summarize that the regularization implementations require a free parameter tuning for a proper trade-off between the error estimation and the overfitting to noisy measurements, which is closely related to the conventional bias-variance equalization. Several works have aimed to give principled recommendations on which of them are more convenient, mostly based on the comparative evaluation of simulations with known solutions [12], [13]. However, and according to the literature, there is no clear consensus in this direction when applying regularization in current commercial systems [5], [7], [14].

In contrast, the implications of regularization tuning have been widely scrutinized and widely described in terms of empirical risk, structural risk, and actual risk, especially as it relates to machine learning [15], [16]. Nevertheless, very few studies implement out-of-sample strategies to adjust the regularization in ECGI estimators, even in simulations with known solution. This could be due in part to the structure of the transmission matrix that relates the measured potentials to the unknowns, as well as the coupled dependency among all these spatio-temporal registers [17]. In this direction, we propose a signal model for inverse cardiac estimation, based on Tikhonov-type regularization and taking advantage of potential superposition properties. This implementation is proved here to increase generalization capabilities for estimating source potentials.

To do this, in this work we propose an implementation of the Tikhonov regularization which is adjusted through cross validation. Experiments performed on signal databases with known solutions and on torso tanks from the EDGAR (Experimental Data and Geometric Analysis Repository) database [18]–[21] yielded significant improvements in terms of error stability. At the same time, the implemented algorithms avoid overfitting by properly managing the error reduction process during the training phase, thus improving the generalization capabilities of cardiac inversion algorithms.

This paper is organized as follows. Section II presents a brief review of the applicable biophysical equations, including the general statement of the inverse problem and the transfer matrices. Subsequently, we introduce the most significant regularization methods used in the literature, together with a justifying development of the superposition principle and the out-of-sample procedure applied in cross-validation. Section III presents simulated in-silico potential estimation experiments with known solutions, together with real applications on experimental data over torso-tank configurations and animal

models [18], [19]. Finally, Section IV summarizes the discussion and Section V conveys the main conclusions of this work.

II. BIOELECTRIC MODEL AND GENERALIZATION EQUATIONS

In this section, we start by reviewing two widely known aspects of the cardiac inverse problem. First, examples of the bioelectric equations are summarized, in a specific form that matches the source potentials with the potentials registered on the torso. It is necessary to mention here that although this is implementation specific, and different formulations could be defined in another way, the presented architecture does not offer loss of generality to solve the inverse cardiac problem. Direct formulations or advanced procedures, such as the Boundary Element Method (BEM) [22], [23], are currently used to convert the problem into an estimation based on matrices and vectors. Also, in this section we briefly review this type of equations for some of the most widely used regularization methods in this setting. Finally, we build on the Potential Superposition Theorem, together with fundamental quasielectrostatic equations, to propose a principled procedure for using out-of-sample generalization strategies in addition to some of the regularization procedures, with an emphasis on the Tikhonov regularization. The latter represents the main contribution of the present work, since it could offer an off-the-shelf and ready-to-use method to be applied to a wide variety of cardiac inverse problem formulations, both in current research and in actual commercial systems.

A. Matrix Notation and Regularization

The well-known equations of a finite inhomogeneous volume conductor can be approached using the Green's Theorem [24], [25]. For a homogeneous medium with a single conductivity σ_0, the equation for its spatial signal model [24] is

$$v_0(\mathbf{r}) = \frac{1}{4\pi\sigma_0} \int_{S'_0} \frac{\nabla^2 v_s(\mathbf{r}')}{|\mathbf{r} - \mathbf{r}'|} dS'_0 \qquad (1)$$

where $\mathbf{r}$ ($\mathbf{r}'$) denotes the position vector of a field point (of a source point), σ_0 is the medium conductivity, v_0 is the potential field under homogeneous conditions, and v_s is the source potential at the immediate S_0 boundary of the transmembrane source currents, for instance, at the epicardial sources.

In a more general case, the volume that constitutes the conducting object is bounded by the torso, by the heart surfaces, and by other anatomical regions, and it is assumed to consist of subregions bounded by closed surfaces, the interior of which has constant conductivity. We denote by S_j the boundary surface that separates two different volumes with their internal and external conductivities being σ_j^i and σ_j^o, respectively, and we assume J different regions with possibly different conductivities. The problem is often expressed as

$$\frac{\sigma_k^i + \sigma_k^o}{2} v_e(\mathbf{r}) = \sigma_0 v_0(\mathbf{r}) - \sum_{j=1}^{J} \frac{\sigma_j^i - \sigma_j^o}{4\pi} \int_{S'_j} v_e(\mathbf{r}') d\Omega'_j \quad (2)$$

where σ_k^i and σ_k^o are the internal and external conductivities in the bounded surface k where the potential is calculated, and the corresponding differential solid angle $d\Omega$ is integrated for each surface [25]. At this point, the application of the BEM

method allows a discretized formulation in matrix form, thus providing an explicit solution for the estimation of the potential. This strategy can be used in the same way to estimate epicardial or transmembrane potentials.

Several steps are taken together for this purpose [22], [26], including spatial discretization of meshed surfaces, integral discretization, and corresponding solid angle calculations based on surface triangles. The potential source $v_s(\mathbf{r})$ is directly embedded in the term of the homogeneous medium response in (2), and it is the unknown information to be retrieved by inverse cardiac estimators. The measurements are assumed to be known on one of the surfaces, in this case $v_e(\mathbf{r})$ over S_k, and the sum of the integrals are obtained over potential field $v_e(\mathbf{r})$ constrained to their value on the heterogeneous surface boundaries, S_j. After discretization of the surfaces and integrals, we obtain a matrix problem in which the primary unknowns are on the source surface, the potential is known on the measured surface, and the set of unknown potentials on the secondary surfaces can be embedded into the system matrix, so that a single transfer matrix is obtained.

Let us denote the set of measurements in a potential-based model consisting of N_e potentials on a given surface as a vector,

$$\mathbf{v}_f = [v_e(\mathbf{r}_1), v_e(\mathbf{r}_2), \ldots, v_e(\mathbf{r}_{N_e})]^\top, \qquad (3)$$

and similarly, let us denote the unknown target potentials on the source surface when measured on its discretized mesh of N_s points on the epicardium also as a vector,

$$\mathbf{v}_s = [v_s(\mathbf{r}'_1), v_s(\mathbf{r}'_2), \ldots, v_s(\mathbf{r}'_{N_s})]^\top, \qquad (4)$$

where we assume that the locations for the measurement mesh nodes of (the source) are known and given by $\mathbf{r}_j$, with $i = 1, \ldots N_e$ (by $\mathbf{r}'_j$, with $j = 1, \ldots N_s$). As explained, the sub-regions with heterogeneous conductivities are measured and discretized, in such a way that the boundary conditions, the geometry, the interpolating basis functions if used, and the biophysical problem, are finally condensed and summarized in a transfer matrix $\mathbf{H}$, with size $N_e \times N_s$, so expressions like (2) can be expressed generally as

$$\mathbf{v}_f = \mathbf{H}\mathbf{v}_s. \qquad (5)$$

This equation should not be solved directly, because measurement errors and uncertainties need to be taken into account, so we can use instead a stochastic version of the above equation, given by

$$\mathbf{v}_f = \hat{\mathbf{v}}_f + \mathbf{e} = \mathbf{H}\hat{\mathbf{v}}_s + \mathbf{e}, \qquad (6)$$

where the hat operator denotes estimated vectors and vector $\mathbf{e}$ represents the noise of the data model.

Several methods have been proposed for estimating the source potentials from the measured potentials after this point, and we summarize here only a few representative ones. Least Squares is a method used for regression in overdetermined systems, and it consists of minimizing the squared sum of the residuals for all the measurements, which in our case can be expressed as

$$\hat{\mathbf{v}}_s = \arg\min_{\mathbf{v}_s}\{\|\mathbf{v}_f - \mathbf{H}\mathbf{v}_s\|^2\}, \qquad (7)$$

and the solution can be readily shown to be

$$\hat{\mathbf{v}}_s = \left(\mathbf{H}^\top\mathbf{H}\right)^{-1}\mathbf{H}^\top\mathbf{v}_f. \qquad (8)$$

However, this approach can represent an ill-conditioned problem, as far as small measurement errors can dramatically distort the estimated source potentials. This may be due in part to smooth variations of the transfer function from two nearby source points, which may provide similar rows at the corresponding locations of the transfer matrix, with the matrix being close to singular. Several procedures have been proposed to compensate for this undesired effect, which are known globally as regularization methods, and we summarize here two of them that are among the most used ones in the field.

1) Tikhonov regularization: is a family of methods to stabilize ill-posed and ill-conditioned problems, which consists of adding a smoothness term to the functional to be minimized [27], [28]. This can be stated as follows,

$$\hat{\mathbf{v}}_s(\gamma) = \arg\min_{\mathbf{v}_s}\left\{\|\mathbf{v}_f - \mathbf{H}\mathbf{v}_s\|^2 + \gamma\|\mathbf{R}\mathbf{v}_s\|^2\right\}, \qquad (9)$$

where γ can be seen as a trade-off parameter between data fit and solution smoothness, and it can be easily shown that such a solution in closed form is

$$\hat{\mathbf{v}}_s(\gamma) = \left(\mathbf{H}^\top\mathbf{H} + \gamma^2\mathbf{R}^\top\mathbf{R}\right)^{-1}\mathbf{H}^\top\mathbf{v}_f. \qquad (10)$$

Matrix $\mathbf{R}$ represents the regularization operator for different orders, in such a way that when $\mathbf{R}$ is the identity matrix we obtain the zero-order Tikhonov (ZOT) regularization, and when $\mathbf{R}$ represents the gradient or the Laplacian operator, we call it first-order and second-order regularization, respectively [29].

Note that free parameter γ has to be set to a suitable value. We could think of minimizing the approximation error to the measured potentials, which would be given by an optimal regularization parameter determined as follows,

$$\gamma^* = \arg\min_{\gamma}\left\{\|\mathbf{v}_f - \hat{\mathbf{v}}_f(\gamma)\|^2\right\}. \qquad (11)$$

However, this criterion itself, called here the Naïve method, will be severely limited, as far as reducing the trade-off parameter will always lead to reduced measurement residual power. But it also will reduce the smoothing effect of the regularization term on the solution, and for small values of γ we will get overfitted solutions that fit extremely to the noisy measurements but not necessarily to the source potentials.

2) TSVD: has also been proposed [30], [31] aiming to overcome the ill-posing character of signal models like the one in (6). To do this, TSVD uses a better defined transfer matrix than $\mathbf{H}$, denoted by $\mathbf{H}_k$. This matrix $\mathbf{H}_k$ is the reconstruction of $\mathbf{H}$ using the k eigenvectors corresponding to the k largest eigenvalues of the Singular Value Decomposition of the transfer matrix. We can express the transfer matrix as follows,

$$\mathbf{H} = \mathbf{U}\mathbf{\Sigma}\mathbf{V}^\top, \qquad (12)$$

where $\mathbf{U}$ and $\mathbf{V}$ are orthogonal matrices, $\mathbf{\Sigma}$ denotes a diagonal matrix, the elements of which are nonnegative reals and denoted as $[\sigma_1, \sigma_2, \sigma_3, \ldots \sigma_{N_e}]$, and they are assumed to be in descending order [32]. Thus, for a given integer $k \leq \text{rank}(\mathbf{H})$, the rank-$k$

reconstruction matrix $\mathbf{H}_k$ can be written as follows,

$$\mathbf{H}_k = \mathbf{U}_k \mathbf{\Sigma}_k \mathbf{V}_k^\top, \tag{13}$$

where $\mathbf{U}_k$ and $\mathbf{V}_k$ are the left and right matrices with the first k singular vectors of $\mathbf{U}$ and $\mathbf{V}$, respectively, and $\mathbf{\Sigma}_k$ is a matrix with the first k singular values of $\mathbf{\Sigma}$. By using these rank-k matrices, the pseudoinverse of $\mathbf{H}_k$ can be computed as

$$\mathbf{H}_k^\dagger = \mathbf{V}_k \mathbf{\Sigma}_k^{-1} \mathbf{U}_k^\top. \tag{14}$$

By following this path, the final result for our estimator can be expressed as

$$\mathbf{v}_s = \mathbf{H}_k^\dagger \mathbf{v}_f = \mathbf{V}_k \mathbf{\Sigma}_k^{-1} \mathbf{U}_k^\top \mathbf{v}_f. \tag{15}$$

Since this method is based on the SVD, the regularization term is defined as the number of singular values used (k), often called the truncating parameter. We could also think of adjusting to its optimum according to

$$k^* = \arg\min_k \|\mathbf{v}_f - \hat{\mathbf{v}}_f(k)\|^2, \tag{16}$$

where efficient approaches for computing these optimal low-rank matrices have been proposed [33].

3) The L-curve method: has been proposed as an alternative to avoid optimization limitations in the Tikhonov's method (e.g., see [34]–[36]). It represents an operational method to determine a suitable regularization parameter, and it is based on plotting the regularization term with respect to the fit term for different values of γ parameter, this is, we plot a two-dimensional scatter plot for the two-dimensional points obtained by

$$\left[\|\mathbf{v}_f - \hat{\mathbf{v}}_f(\gamma)\|^2, \|\mathbf{R}\hat{\mathbf{v}}_s(\gamma)\|^2 \right] \tag{17}$$

and according to different values of γ on a logarithmic scale in (10). This resulting curve typically has an L-shape, and the elbow can be shown to correspond to an optimal value for the regularization parameter, as far as it represents a balance between the two terms (adjusting and smoothing). The elbow is considered to give us the largest possible parameter corresponding to the estimation of the potentials without approximating the measurement noise too closely. Note that the L-curve is not a regularization method itself, but rather it represents a graph-based procedure that aims to find a suitable value for the regularization parameter and for a given regularization method.

B. Superposition and Out-of-Sample Generalization

The regularization methods described above can sometimes have instabilities or give apparently inconsistent solutions. For example, a wide range of searched values for parameter γ in Tikhonov may work well for some signal snapshots, but not so well for other snapshots. To some extent, it can be thought that this is related to an implementation that does not adequately deal with the trade-off between bias and variance and, as a consequence, the regularization term cannot guarantee generalization capabilities.

The trade-off between the approximation error and the estimator complexity in terms of generalization properties has been intensely studied in the field of machine learning. Specifically, the description of estimating machines and their complexity

in terms of empirical risk, structural risk, and actual risk, is a basic but powerful framework for analyzing a wide variety of estimators, as seen in [15], [16] for the theoretical fundamentals and for the application of bootstrap resampling in cardiac arrhythmia discrimination problems, respectively. For a given data learning scheme, the empirical risk is related to the observed errors in the data used to build the model coefficients, while the structural risk is related with the possible complexity of the learning functions. The actual risk is a combination of both, such that for a given learning machine, increasing the complexity often reduces the empirical risk, but the actual risk (i.e., the sum of both terms) has an optimal complexity-error trade-off, which is the optimal working point to obtain the best possible generalization properties for a given free parameter. In those cases where the structural risk is not easy to characterize mathematically (for example, using the Vapnik-Chervonenkins dimension of the machine as in some kernel methods [16]), an operational option to characterize the actual risk consists of evaluating the prediction error on some set of observations that are not involved with fitting the model weights, which we will call here out-of-sample observations. It is well known that this corresponds to the use of training sets and validation sets of data in many machine learning problems, where the observations are assumed to be independent and identically distributed [37].

Our proposed implementation considers an out-of-sample procedure to establish the best possible generalization properties by including a regularization term and using the Superposition Principle. The model also includes all the necessary considerations to cope with singularities at the interface surfaces of the volumes, caused by the differences in the conductivities of the separated elements. (2) shows an example that incorporates the activation of a series of secondary sources, which are electrostatically closely linked to the primary sources (for a more detailed description, see [24]). Now, using the Superposition Principle, the potential can be obtained as the aggregation of all the individual source nodes of surface S_0. The next step is to apply the cross validation through successive subsampling of the total activity of the nodes, which is expected to be a valid consideration for the field estimation in S_k, especially when the full set of measurements is large enough. Fig. 1(a) depicts a schematic for this approach, and Fig. 1(b) shows the split of the cross-validation set inside and outside the sample on a real case. In particular on the torso, dots are colored according to the set to which each field potential measurement belongs, namely, yellow if the electrode belongs to the in-sample subset and magenta if it belongs to the out-of-sample subset. Fig. 1(c) shows a representation of the proposed algorithm. The torso electrodes are split into the same structure, in-sample and out-of-sample electrodes, using the mentioned color pattern. Then, by using a $\mathbf{H}$-matrix reduction ($\mathbf{H}^i$) which maps the in-sample field (torso) electrodes to cavity (source) potential points, the source potentials are estimated. Finally, by using another $\mathbf{H}$ submatrix ($\mathbf{H}^o$), which maps all the source potentials to the out-of-sample field potentials, the direct problem is solved. The out-of-sample estimated field potentials allow to build the model error based on a set of observations which are not used to build the model coefficients, thus improving their actual inference capabilities.
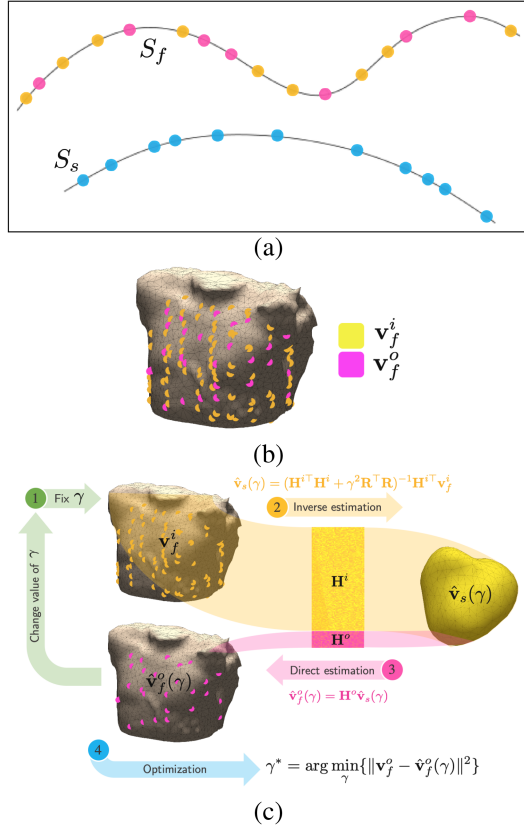
Fig. 1. Draft of the bioelectric out-of-sample strategy. In (a), we want to estimate potentials on surface S_s at the blue point locations with available measurements in surface S_f. For a given value of a free parameter, we solve with only the yellow points at S_f, and evaluate the actual risk on the magenta points at S_f. (b) Schematic of the in-sample and out-of-sample set split over an example in a real torso. (c) Schematic of the out-of-sample strategy over the example torso and cavity model from EDGAR database.

Algorithm 1: Out-of-sample pseudo-code algorithm.

Input: $\mathbf{v}_f$, $\mathbf{H}$, $\mathbf{R}$, I as field potential in-of-sample indices, and O as field potential out-of-sample indices.
Output: $\hat{\mathbf{v}}_s$.
1: $\mathbf{H}^i \leftarrow$ rows of $\mathbf{H}$ corresponding to I.
2: $\mathbf{H}^o \leftarrow$ rows of $\mathbf{H}$ corresponding to O.
3: $\mathbf{v}_f^i \leftarrow$ torso voltage $\mathbf{v}_f$ corresponding to I.
4: $\mathbf{v}_f^o \leftarrow$ torso voltage $\mathbf{v}_f$ corresponding to O.
5: **for** γ **do**
6: $\quad \hat{\mathbf{v}}_s(\gamma) = (\mathbf{H}^{i\top}\mathbf{H}^i + \gamma^2\mathbf{R}^\top\mathbf{R})^{-1}\mathbf{H}^{i\top}\mathbf{v}_f^i$, see (10)
7: $\quad \hat{\mathbf{v}}_f^o(\gamma) = \mathbf{H}^o\hat{\mathbf{v}}_s(\gamma)$, see (21)
8: **end for**
9: $\gamma^* = \arg\min_\gamma\{\|\mathbf{v}_f^o - \hat{\mathbf{v}}_f^o(\gamma)\|^2\}$, see (22)
10: $\hat{\mathbf{v}}_s = (\mathbf{H}^\top\mathbf{H} + \gamma^{*2}\mathbf{R}^\top\mathbf{R})^{-1}\mathbf{H}^\top\mathbf{v}_f$, see (10)

The γ value is selected to minimize the assessed error relating real field potentials and estimated field potentials. Algorithm 1 also shows the whole flow to perform the out-of-sample strategy over a torso-cavity system if the torso voltage and the transfer matrix are known.

Therefore, a partition of the observed measurements can be done, which we will call in-sample and out-of-sample, which in vector form can be expressed as

$$\mathbf{v}_f = \begin{bmatrix} \mathbf{v}_f^i \\ \mathbf{v}_f^o \end{bmatrix}, \tag{18}$$

where the observations have been assigned randomly to one or another subset, and N_e^i (N_e^o) is the number of in-sample (out-of-sample) observations. Now, the problem can be expressed in matrix-vector form as follows,

$$\begin{bmatrix} \mathbf{v}_f^i \\ \mathbf{v}_f^o \end{bmatrix} = \begin{bmatrix} \mathbf{H}^i \\ \mathbf{H}^o \end{bmatrix} \mathbf{v}_s. \tag{19}$$

Hence, we obtain the following uncoupled matrix equations:

$$\mathbf{v}_f^i = \mathbf{H}^i\mathbf{v}_s \tag{20}$$

$$\mathbf{v}_f^o = \mathbf{H}^o\mathbf{v}_s \tag{21}$$

and now, the first equation can be used to adjust the estimation weights according to a given regularization parameter, while the second one can be used to yield the actual risk measured in the out-of-sample potentials. Note that regularization matrices $\mathbf{R}$, as well as other elements of regularization schemes, could need some adjustment to the partition made for the out-of-sample determination.

The above approach allows us to elaborate on several quasi-electrostatic potential signal models and on the estimation algorithms and regularization methods used on them to establish an out-of-sample criterion, thus obtaining a good-quality regularization parameter tuning and improving the generalization capabilities in cardiac inverse problems. For instance, the use of Tikhonov regularization can be addressed with well-known methods, such as cross validation and V-folds validation. The cross-validation method [38] is often used in machine learning algorithms, and it consists in just splitting the observed dataset into a training subset and a validation subset. The simplest validation strategy consists of using about 60-90% of the observations for model weight adjustment and the others for out-of-sample validation. In our case, we can rewrite (10) as follows:

$$\gamma^* = \arg\min_\gamma\left\{\|\mathbf{v}_f^o - \hat{\mathbf{v}}_f^o(\gamma)\|^2\right\}, \tag{22}$$

where superscript * indicates the optimum obtained through the out-of-sample procedure. Once obtained the optimum parameter, it is used with the full set of samples, for better generalization capabilities. Note that we can also think of making a similar partition on the regularization matrix,

$$\mathbf{R} = \begin{bmatrix} \mathbf{R}^i \\ \mathbf{R}^o \end{bmatrix}. \tag{23}$$

So, the solution for (11) is given instead by solving for each gamma,

$$\hat{\mathbf{v}}_s(\gamma) = \arg\min_{\mathbf{v}_s}\left\{\|\mathbf{v}_f^i - \mathbf{H}^i\mathbf{v}_s\|^2 + \gamma\|\mathbf{R}^i\mathbf{v}_s\|^2\right\}, \tag{24}$$

which gives the solution to the estimation problem.

Other elaborated out-of-sample schemes can be followed, such as V-folds [39], which consists of dividing the complete set of observations into V subsets, and in each iteration we use $V-1$ subsets for weight adjustment and the remaining for out-of-sample characterizations. The V estimations of the actual risk are averaged to give the final estimation. Finally, note that also L-curve and TSVD methods could also be reformulated from this approach.

III. EXPERIMENTS AND RESULTS

This experimental section is divided into two parts. On the one hand, simple cases are implemented and analyzed to achieve a better understanding of the out-of-sample strategy in simulation problems with known solutions. In the second one, we move to real situations through the EDGAR database to scrutinize the improvement in the generalization capabilities of the out-of-sample strategy on real datasets.

Three estimation methods were implemented. In the Naïve method, γ is adjusted for ZOT regularization by minimizing the error in the $\mathbf{v}_e$ measured potentials (extracellular and torso). The L-curve is also applied according to the recommendations generally followed in [40]. Finally, the 2-folds cross validation represents and implements the out-of-sample strategy proposed here to adjust free parameter γ in ZOT regularization. Note that the Naïve method is not used in practice, but it is included here to better analyze overfitting situations that may be present.

The L-curve is the most widely used method in current literature, although here we do not consider implementation variations among different authors. We limit ourselves to analyzing the out-of-sample strategy in a Tikhonov example and not in all Tikhonov variants or in TSVD, although it can be easily verified that they exhibit qualitatively similar behavior. The values of γ analyzed were selected in synthetic cases with a 30-point logarithmic grid from 10^{-10} to 10^3, and in real cases from the EDGAR database with a 30-point logarithmic grid from 10^{-10} to 1. To compare accuracy, we obtained Pearson's correlation coefficient (ρ) and root mean squared error (RMSE), given by

$$\rho = \frac{cov(\mathbf{u}, \hat{\mathbf{u}})}{\sigma_{\mathbf{u}}\sigma_{\hat{\mathbf{u}}}}; \quad RMSE = \sqrt{\frac{1}{N}\|\mathbf{u} - \hat{\mathbf{u}}\|^2} \quad (25)$$

where $cov()$ is the covariance operator and $\sigma_{\mathbf{u}}$ is the standard deviation of vector $\mathbf{u}$, this representing either $\mathbf{v}_e$ or $\mathbf{v}_s$.

A. Simple Simulated Cases

Two different known-solution cases were simulated, namely a cylinder (representing fast depolarization) and a Gaussian pulse (representing repolarization) stimulus on transmembrane voltage on a planar substrate. All these simulations were carried out on a uniform cell substrate of 45×45. The supplementary material shows details on the calculation of $\mathbf{H}$ matrix in this experiment, as well as the Laplacian operator for this set of experiments and additional information. We compared noise-free measurements with both the field potentials and the $\mathbf{H}$ matrix within additive white Gaussian noise of 20 dB of signal-to-noise ratio (SNR).
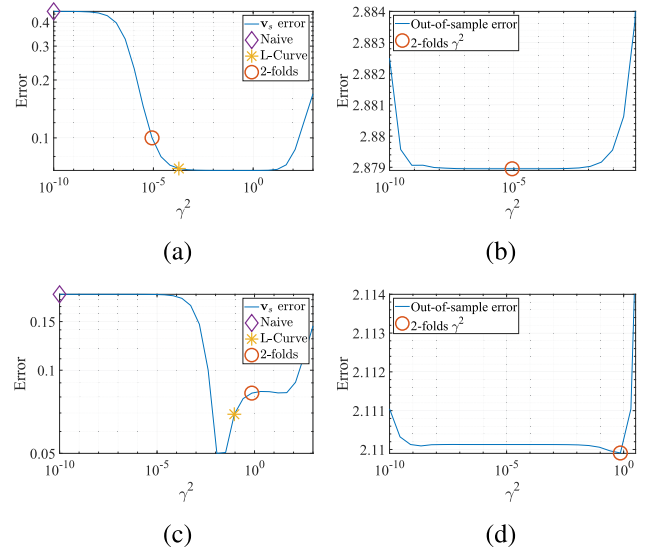

Fig. 2. Estimation errors as a function of parameter γ^2: (a), (c) Estimation error for the source potentials, with markers for the different methods; (b,d) Detailed out-of-sample error for 2-folds method (blue) and selected γ (red); (a), (b) Noise-free cylindrical pulse; (c), (d) Noisy Gaussian pulse.

Note that $\mathbf{v}_f$ in (3) and (6) refers to potentials measured through electrodes, while $\mathbf{v}_s$ refers to source potentials, to be estimated. For example, $\mathbf{v}_f$ could refer to the measured torso potentials and $\mathbf{v}_s$ to the epicardial potentials to be estimated, as usual in ECGI. But also $\mathbf{v}_f$ could refer to intracardiac potentials measured from floating electrodes inside a cardiac chamber and $\mathbf{v}_s$ could refer to their corresponding extracellular potentials in the endocardium. And also $\mathbf{v}_f$ could refer to endocardial potential measurements from electrodes and $\mathbf{v}_s$ could be the endocardial transmembrane potential to be estimated. The simulated case in this experiment corresponds to the third example above, whereas the cage examples from Utah and the in vivo one from Maastricht in the next experiment refer to the first example above.

Fig. 2 shows the complete estimation error curves as a function of γ^2 parameter. The known-solution error for the source potentials can be observed in these cases, showing a wide range of values working correctly, though this range becomes narrower in the presence of noise. We can verify that the free parameter selected with the 2-folds is acceptable but close to the limit of the wide working zone, whereas the L-curve parameter is close to absolute optimum. These results, together with the tables and details on the supplementary materials, show that the proposed method can estimate the source potential with an error close to that computed with the L-curve method. For this reason, it is necessary to obtain the behavior of the proposed method on different real datasets.

B. Examples From EDGAR

Additional sets of experiments were developed by using real bioelectric signals from the EDGAR Time Signal Catalog [21]. The first selected dataset was for the ischemia torso tank with a
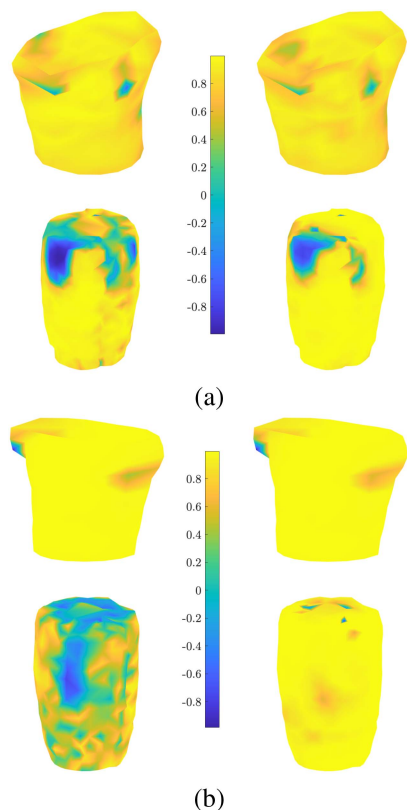
Fig. 3. Accuracy spatial distributions for the Utah torso tank examples, when using L-curve (left) and 2-folds method (right). (a) Map of correlation coefficients between the torso signals and their estimations (up) and the measured and estimated electrograms (down) for the control case. (b) The same for the intervention case.
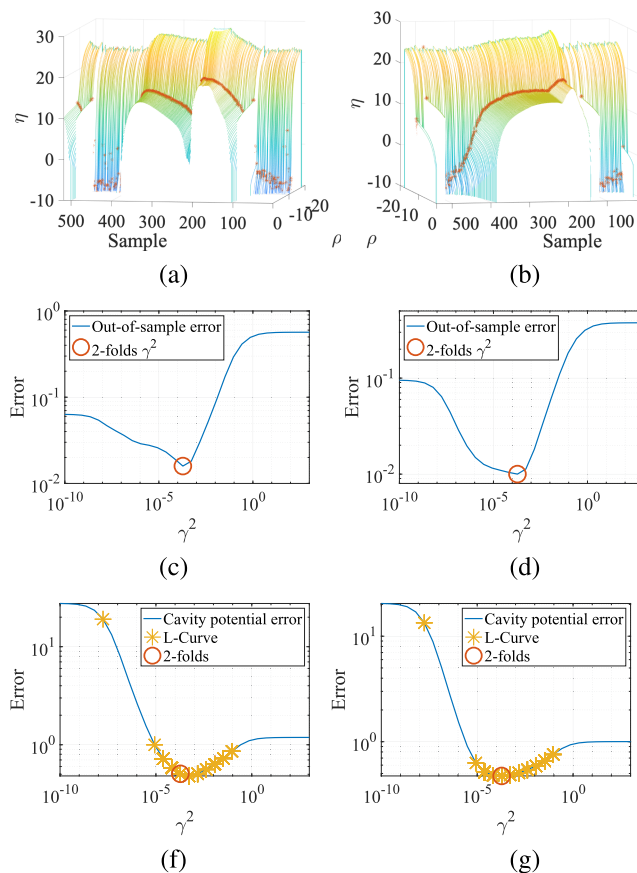

Fig. 4. Details on the free parameter tuning for each analyzed method. (a), (b) L-curve computation for the two Utah cases at each time instant, with the selected elbow points in red. (c), (d) Detailed out-of-sample error for 2-folds method (blue) and selected γ (red). (f), (g) Estimation error with γ^2 values selected from L-curve at each time instant (yellow) and with 2-folds (red).

cardiac cage, obtained and publicly shared by the Cardiovascular Research and Training Institute and the Scientific Computing and Imaging Institute from Utah University [41]. This dataset consists of 4 different subsets, namely a control subset plus three intervention subsets, each consisting of several records on the torso and cavity geometries, and a transfer matrix $\mathbf{H}$ with size 192×599. The torso signal recordings consisted of 192 from Body Surface Potential Mapping (BSPM) sensor signals, while the cavity records consisted of 599 needle sensor signals, which are known as Electrogram (EGM), connected to the cage. We present here the results for each record in this dataset focusing on two selected cases given by record 0003 from the control subset and record 0033 from the intervention dataset. Supplementary material includes additional results from this dataset and the description and additional results for the second dataset from EDGAR (Maastricht dataset).

Relevant insights can be obtained for the Utah examples from Fig. 3, which shows the spatial distribution of ρ for each surface and each case and each method (the yellower, the better). We can check again that the torso potentials are in good agreement for all cases in terms of this merit figure. For the control record, we can observe regionalized drops of estimation quality on the cage (sources) with L-curve, which are also present in 2-folds, but much more moderated and in a smaller region. For the ischemia

record, the estimation quality for L-curve drops on all the source surface, whereas it slightly decreases at some regions with the proposed out-of-sample strategy.

Moreover, Fig. 4(a,b) shows the L-curve from control and third intervention recordings from the Utah dataset, noting that each curve represents a temporal sample, as often implemented in this method for ECGI calculations. As it can be seen in the subsequent panels for the in-sample and for the out-of-sample estimation errors, there is noticeable variability for the estimation of the elbow position, which corresponds to widespread extended values of each time snapshot compared with the averaged optimal behavior as pointed by the out-of-sample criterion. This indicates that sometimes the L-curve will work well, but others it can give inaccurate estimations and errors due to this variability. Furthermore, Fig. 5(a) shows the RMSE value for each recording from Utah dataset. As it can be seen, RMSE values are very similar in most of the recordings, but in the first five of them the out-of-sample method achieves better performance, which evidences the estimation variability of the L-curve in some examples. A similar behavior can be observed in Fig. 5(b), where the performance of each method is shown in terms of ρ.
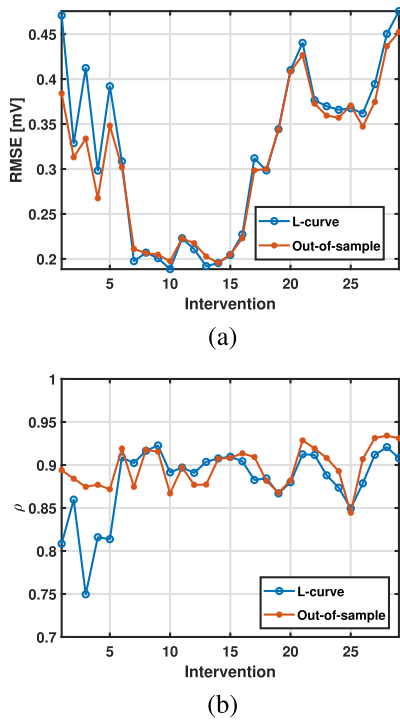
(a)

(b)

Fig. 5.   Behavior of L-curve, blue, and out-of-sample, red, for each record in Utah dataset. (a) Behavior in terms of RMSE. (b) Behavior in terms of ρ.

IV. Discussion

A new framework has been proposed to estimate the regularization parameter in cardiac potential estimation problems. Generalization capabilities are reinforced by using a data partition, following well-known machine learning principles.

On the one hand, the out-of-sample methods, as cross-validation or others including leave-one-out or V-folds, may give a working range for the free parameter. We have assumed here that this free parameter is adequate when using all the samples at the final step. On the other hand, sometimes the case examples represented were obtained with pacing, so the stimulation spike is visible at a given time before and after the beat. When the L-curve fails to provide an adequate tuning for the free parameter, the spike can be strongly distorted. Whereas this does not imply a problem *per se*, as far as the spike can be easily recognized and it has no diagnostic information for the clinician, it shows that severe distortion can be affecting the high-frequency components of the signals under these conditions.

The clinical usefulness of ECGI systems is growing in our days. Rudy made an extensive review on the works from his lab and others on ECGI capacities in arrhythmogenic substrates linked with clinical arrhythmias, covering heart failure, myocardial infarction, atrial fibrillation, and abnormal ventricular repolarization, among many others [3]. This review was later extended [4] towards clinical success cases on providing the clinicians with useful information on patients with hereditary arrhythmogenic syndromes (specifically, long QT and Brugada syndromes), by following similar noninvasive approaches for mapping the electrophysiological substrate of post-infarction

myocardial scars and relating it with the activation patterns during reentrant ventricular tachycardias. Several commercial systems have emerged which are been currently evaluated with advantages [42], [43].

The clinical validation of ECGI systems has dramatically advanced in recent years, despite not being a trivial task. Other studies have supported this clinical usefulness from experimental setups, for instance, Langendorff-perfused pig hearts were suspended in a human-shaped torso tank in [44], where cardiac EGMs were recorded with a 108-electrode sock and torso signals were measured with 256 electrodes embedded in the tank surface. EGMs were noninvasively reconstructed, and estimated activation and repolarization features were compared to those recorded ones, validating a potential ECGI-based approach to noninvasively image activation and recovery in sinus rhythm. Despite some reported inaccuracies in epicardial breakthroughs and lines of conduction block, other relevant clinical features, such as abnormal repolarization regions, were derived from ECGI recordings. Probably related with the increased use of ECGI in clinical environments, some controversial results are occasionally obtained. A recent study aimed to evaluate the ECGI in clinical conditions [7], and for this purpose, the accuracy of activation maps from this system was evaluated in 55 patients from which epicardial maps were recorded with catheters in electrophysiological study. The correlation between both activation maps had limited quality, and more, low-voltage areas as well as septal signals were found to be also limiting. On the other hand, the correlation was higher in patients with wide QRS complex (due either to stimulation or to bundle branch block). While authors sustained that activation maps in ECGI are useful for ectopic beats or pacing, but not for sinus rhythm, responses from other groups [14] stated that the observed differences might be due to operation or algorithmic suboptimal handling. The possible use of ECGI in ablation guidance for atrial fibrillation has received special attention in recent years, as seen in [5] for a recent review on this topic where limitations and future directions are identified and proposed.

To our best knowledge, few out-of-sample implementations ensuring the generalization when using regularization techniques can be found in the ECGI literature. The Generalized Cross Validation Method proposed and used in [45], [46] used a criterion on the change of behavior of an L-curve. A recent study was devoted to analyze with detail the impact of signal processing techniques on the reconstructions of single-site pacing data on a torso-tank experimental setup [47], which mostly used elbow detection on the L-curve. Other studies proposing additional approaches in some setting also used elbow profiling [48]–[51]. The excellent review of the ECGI techniques by Gulrajani [52] stated that in general it is enough to retain the lowest regularization parameter which makes the solution stable. Instead, and as explained in the preceding sections, we conclude here that the use of out-of-sample approaches following well-known principles in machine learning [15], [16], [53] can improve and stabilize the solutions of inverse cardiac problems. The extension of the current application is expected to move towards other spatial-temporal signal models and to other regularization techniques and scenarios.

V. CONCLUSION

We have proposed a signal model aiming to provide a principled support to out-of-sample implementations of regularization techniques in inverse cardiac problems. Grounded on the Potential Superposition Principle, a partition can be made on the measurements that allows to estimate the cardiac sources while evaluating the actual risk on independent subsets of measurements. The approach has been tested for simulated and real data and it can provide a methodological support for determining stable free parameter values in Tikhonov regularization. As far as the Superposition Principle can be assumed in the signal model equations, it can be extended to other inverse cardiac problems (estimation of transmembrane potentials, of epicardial potentials, or of endocardial potentials, for instance), as well as to other regularization approaches.

REFERENCES

[1] World Health Organization, "The top 10 causes of death," Accessed: Feb. 10, 2022. [Online]. Available: https://www.who.int/news-room/fact-sheets/detail/the-top-10-causes-of-death

[2] GBD 2013 Mortality and Causes of Death Collaborators, "Global, regional, and national age-sex specific all-cause and cause-specific mortality for 240 causes of death, 1990–2013: A systematic analysis for the global burden of disease study 2013," *Lancet*, vol. 385, no. 9963, pp. 117–171, 2015.

[3] Y. Rudy, "Noninvasive electrocardiographic imaging ECGI of arrhythmogenic substrates in humans," *Circulation Res.*, vol. 112, no. 5, pp. 863–874, 2013.

[4] Y. Rudy, "Noninvasive ECG imaging (ECGI): Mapping the arrhythmic substrate of the human heart," *Int. J. Cardiol.*, vol. 237, no. 1, pp. 13–14, 2017.

[5] J. Salinet *et al.*, "Electrocardiographic imaging for atrial fibrillation: A perspective from computer models and animal experiments to clinical value," *Front. Physiol.*, vol. 12, 2021, Art. no. 653013.

[6] C. Andrews *et al.*, "Electrical and structural substrate of arrhythmogenic right ventricular cardiomyopathy determined using noninvasive electrocardiographic imaging and late gadolinium magnetic resonance imaging," *Circulation Arrhythmia Electrophysiol.*, vol. 10, no. 7, 2017, Art. no. 5105.

[7] J. Duchateau *et al.*, "Performance and limitations of noninvasive cardiac activation mapping," *Heart Rhythm*, vol. 16, no. 3, pp. 435–442, 2019.

[8] H. Pereira *et al.*, "Electrocardiographic imaging for cardiac arrhythmias and resynchronization therapy," *Europace*, vol. 22, no. 10, pp. 1447–1462, 2020.

[9] S. Pagani *et al.*, "Data integration for the numerical simulation of cardiac electrophysiology," *Pacing Clin. Electrophysiol.*, vol. 44, no. 4, pp. 726–36, 2021.

[10] R. Dubois *et al.*, "Non-invasive cardiac mapping in clinical practice: Application to the ablation of cardiac arrhythmias," *J. Electrocardiol.*, vol. 48, no. 6, pp. 966–974, 2015.

[11] P. Maury *et al.*, "Three-dimensional mapping in the electrophysiological laboratory," *Arch. Cardiovasc. Dis.*, vol. 111, no. 6, pp. 456–464, 2018.

[12] A. Karoui *et al.*, "Evaluation of fifteen algorithms for the resolution of the electrocardiography imaging inverse problem using ex-vivo and in-silico data," *Front. Physiol.*, vol. 9, 2018, Art. no. 1708.

[13] C. Figuera *et al.*, "Regularization techniques for ECG imaging during atrial fibrillation: A computational study," *Front. Physiol.*, vol. 7, 2016, Art. no. 466.

[14] Y. Rudy, "Comments on ECGI and activation mapping," *Heart Rhythm*, vol. 16, pp. E50–E51, Jun. 2019.

[15] J. L. Rojo-Álvarez, A. Arenal-Maiz, and A. Artes-Rodriguez, "Discriminating between supraventricular and ventricular tachycardias from EGM onset analysis," *IEEE Eng. Med. Biol. Mag.*, vol. 21, no. 1, pp. 16–26, Jan./Feb. 2002.

[16] V. Vapnik, *Statistical Learning Theory*. New York, NY, USA: Wiley, 1998.

[17] C. Jamison *et al.*, "The inverse problem utilizing the boundary element method for a nonstandard female torso," *IEEE Trans. Biomed. Eng.*, vol. 58, no. 4, pp. 876–883, Apr. 2011.

[18] M. Cluitmans *et al.*, "In vivo validation of electrocardiographic imaging," *J. Amer. College Cardiol.: Clin. Electrophysiol.*, vol. 3 no. 3, pp. 232–242, 2017.

[19] R. MacLeod *et al.*, "Construction of a human torso model from magnetic resonance images for problems in computational electrocardiography," School Comput., Univ. Utah, Salt Lake City, UT, USA, Tech. Rep. UUCS-94-017, 1994.

[20] D. Brooks and R. MacLeod, "Electrical imaging of the heart," *IEEE Signal Process. Mag.*, vol. 14, no. 1, pp. 24–42, Jan. 1997.

[21] K. Aras *et al.*, "Experimental data and geometric analysis repository - EDGAR," *J. Electrocardiol.*, vol. 48, no. 6, pp. 975–981, 2015.

[22] C. Brebbia and J. Dominguez, *Boundary Elements: An Introductory Course*, 2nd ed. Ashurst, Southampton, U.K.: WIT Press, 2012.

[23] SCI Institute, "SCIRun: A. Scientific computing problem solving environment, scientific computing and imaging institute (SCI)," 2016. [Online]. Available: http://www.scirun.org

[24] R. Plonsey and R. Barr, *Bioelectricity: A Quantitative Approach*, 3rd ed. Berlin, Germany: Springer, 2007.

[25] J. Sarvas, "Basic mathematical and electromagnetic concepts of the biomagnetic inverse problem. physics in medicine and biology," *Clin. Cardiol.*, vol. 32, pp. 11–22, 1987.

[26] A. Cheng and D. Cheng, "Heritage and early history of the boundary element method," *Eng. Anal. Boundary Elements*, vol. 29, no. 3, pp. 268–302, 2005.

[27] A. Tikhonov and V. Glasko, "Use of the regularization method in non-linear problems," *USSR Comput. Math. Math. Phys.*, vol. 5, no. 3, pp. 93–107, 1965.

[28] D. Calvetti and L. Reichel, "Tikhonov regularization of large linear problems," *BIT Numer. Math.*, vol. 43, pp. 263–283, Jan. 2003.

[29] B. Bergquist *et al.*, "Novel experimental preparation to assess electrocardiographic imaging reconstruction techniques," in *Proc. Comput. Cardiol.*, 2020, pp. 1–4.

[30] Z. Wu *et al.*, "A new method for TSVD regularization truncated parameter selection," *Math. Problems Eng.*, vol. 11, 2013, Art. no. 161834.

[31] R. Caulier-Cisterna *et al.*, "A new approach to the intracardiac inverse problem using Laplacian distance kernel," *Biomed. Eng. OnLine*, vol. 17, no. 1, 2018, Art. no. 86.

[32] S. Noschese and L. Reichel, "A modified truncated singular value decomposition method for discrete ill-posed problems," *Numer. Linear Algebra Appl.*, vol. 21, pp. 813–822, 2014.

[33] J. Chung and M. Chung, "An efficient approach for computing optimal low-rank regularized inverse matrices," *Inverse Problems*, vol. 30, no. 11, Oct. 2014, Art. no. 114009.

[34] P. Hansen, "Analysis of discrete ill-posed problems by means of the L-curve," *SIAM Rev. I.*, vol. 34, no. 4, pp. 561–580, 1992.

[35] P. Hansen and D. O'Leary, "The use of the L-curve in the regularization of discrete ill-posed problems," *SIAM J. Sci. Comput.*, vol. 14, pp. 1487–1503, 1993.

[36] P. Hansen, *The L-Curve and Its Use in the Numerical Treatment of Inverse Problems*, vol. 4. Ashurst, Southampton, U.K.: WIT Press, Jan. 2001, pp. 119–142.

[37] R. Tibshirani, "Regression shrinkage and selection via the Lasso: A retrospective," *J. Roy. Stat. Soc.: Ser. B. (Statist. Methodol.)*, vol. 73, no. 3, pp. 273–282, 2011.

[38] M. Kuhn and K. Johnson, *Measuring Performance in Classification Models*. New York, NY, USA: Springer, 2013, pp. 247–273.

[39] R. Kohavi, "A study of cross-validation and bootstrap for accuracy estimation and model selection," in *Proc. 14th Int. Joint Conf. Artif. Intell.*, 1995, vol. 2, pp. 1137–1143.

[40] P. Hansen, "Regularization tools: A Matlab package for analysis and solution of discrete ill-posed problems," *Numer. Algorithms*, vol. 6, no. 1, pp. 1–35, Mar. 1994.

[41] J. Tate *et al.*, "Reducing error in ECG forward simulations with improved source sampling," *Front. Physiol.*, vol. 9, 2018, Art. no. 1304.

[42] G. Cheniti *et al.*, "Noninvasive mapping and electrocardiographic imaging in atrial and ventricular arrhythmias (CardioInsight)," *Cardiac Electrophysiol. Clin.*, vol. 11, no. 3, pp. 459–471, 2019.

[43] J. Azpilicueta *et al.*, "ECGI in atrial fibrillation: A Clinician's wish list," *J. Electrocardiol.*, vol. 51, no. 6S, pp. 88–91, 2018.

[44] L. Bear *et al.*, "Advantages and pitfalls of noninvasive electrocardiographic imaging," *J. Electrocardiol.*, vol. 57, pp. S15–S20, 2019.

[45] J. Barnes and P. Johnston, "Application of robust generalised cross-validation to the inverse problem of electrocardiology," *Comput. Biol. Med.*, vol. 69, pp. 213–225, 2016.

[46] P. Johnston, "Accuracy of electrocardiographic imaging using the method of fundamental solutions," *Comput. Biol. Med.*, vol. 102, pp. 433–448, 2018.

[47] L. Bear *et al.*, "The impact of torso signal processing on noninvasive electrocardiographic imaging reconstructions," *IEEE Trans. Biomed. Eng.*, vol. 68, no. 2, pp. 436–447, Feb. 2021.

[48] H. Oster and Y. Rudy, "The use of temporal information in the regularization of the inverse problem of electrocardiography," *IEEE Trans. Biomed. Eng.*, vol. 39, no. 1, pp. 65–75, Jan. 1992.

[49] Y. Serinagaoglu, D. H. Brooks, and R. S. Macleod, "Improved performance of Bayesian solutions for inverse electrocardiography using multiple information sources," *IEEE Trans. Biomed. Eng.*, vol. 53, no. 10, pp. 2024–2034, Oct. 2006.

[50] K. Coleman *et al.*, "Surface unipolar electrogram characteristics to predict site of origin of outflow tract arrhythmias using noninvasive mapping," *J. Cardiovasc. Electrophysiol.*, vol. 32, pp. 391–399, Feb. 2021.

[51] V. Kara *et al.*, "ECG imaging to detect the site of ventricular ischemia using torso electrodes: A computational study," *Front. Physiol.*, vol. 10, 2019, Art. no. 50.

[52] R. M. Gulrajani, "The forward and inverse problems of electrocardiography," *IEEE Eng. Med. Biol. Mag.*, vol. 17, no. 5, pp. 84–101, Sep./Oct. 1998.

[53] G. Golub *et al.*, "Generalized cross-validation as a method for choosing a good ridge parameter," *Technometrics*, vol. 21, no. 2, pp. 215–223, 1979.